Journal of Catalysis 259 (2008) 223–231

Contents lists available at ScienceDirect

Journal of Catalysis

www.elsevier.com/locate/jcat

Catalytic performance of rhodium supported on ceria–zirconia mixed oxides for reduction of NO by propene

Masaaki Haneda [a,*], Kiyoshi Shinoda [b], Akira Nagane [b], Ohki Houshito [b], Hiromitsu Takagi [b], Yuunosuke Nakahara [b], Kazumi Hiroe [b], Tadahiro Fujitani [c], Hideaki Hamada [a]

[a] Research Center for New Fuels and Vehicle Technology, National Institute of Advanced Industrial Science and Technology (AIST), AIST Tsukuba Central 5, 1-1-1 Higashi, Tsukuba, Ibaraki 305-8565, Japan
[b] Mitsui Mining and Smelting Co., Ltd, 1332-2 Haraichi, Ageo, Saitama 362-0021, Japan
[c] Research Institute for Innovation in Sustainable Chemistry, National Institute of Advanced Industrial Science and Technology (AIST), AIST Tsukuba West, 16-1 Onogawa, Tsukuba, Ibaraki 305-8569, Japan

ARTICLE INFO

Article history:
Received 19 June 2008
Revised 20 August 2008
Accepted 21 August 2008
Available online 16 September 2008

Keywords:
NO reduction
Propene
Stoichiometric conditions
Rhodium
Ceria–zirconia mixed oxide
Fourier transform infrared spectroscopy

ABSTRACT

The catalytic activity of $Rh/CeO_2–ZrO_2$ for NO reduction by C_3H_6 under stoichiometric conditions was found to depend strongly on the Ce/Zr composition. $Rh/CeO_2–ZrO_2$ with a Ce/Zr molar ratio of 50/50 (Rh/CZ-50/50) had the greatest activity; Ce/Zr = 74/26 (Rh/CZ-74/26), the least. The Rh/CZ-50/50 also showed specifically high intrinsic activity expressed in terms of turnover frequency (TOF). Different characterization techniques revealed that the Rh and $CeO_2–ZrO_2$ support interaction varied according to Ce/Zr composition, and high TOF on Rh/CZ-50/50 was accounted for by the strong Rh and $CeO_2–ZrO_2$ support interaction. Although the Rh/CZ-74/26 catalyst was the least active, it was able to catalyze NO reduction with C_3H_6 when O_2 was eliminated from the reaction gas. In situ FT-IR spectroscopy suggested that formate species formed and stabilized on the Rh/CZ-74/26 catalyst poison the catalytically active sites for NO reduction with C_3H_6.

1. Introduction

Three-way catalysts (TWCs) represent one of the most innovative technologies for automotive emission control. TWCs can work simultaneously and efficiently to reduce NO and to oxidize CO and hydrocarbons (HC) in a narrow window of air-to-fuel ratio (A/F), close to the stoichiometric point. But under actual operating conditions, the A/F ratio frequently fluctuates between fuel-lean and fuel-rich compositions. With the aim of widening the operational A/F window, cerium oxide-based materials have been used as oxygen storage components to provide oxygen for the oxidation of CO and HC under fuel-rich conditions and to remove oxygen from the gas phase for the reduction of NO under fuel-lean conditions [1]. Of the oxygen storage materials reported so far [2–8], $CeO_2–ZrO_2$ mixed oxides appear to be the best choice for TWC application.

Although oxygen storage materials are key components in TWCs, the catalytically active components in TWCs are precious metals, such as Pt, Pd, and Rh. The total demand for precious metals for automotive catalysts is growing due to increasing environmental awareness [9]. Studies of ways to minimize the use of precious metals are gaining extensive attention as a result.

TWCs often are exposed to high-temperature exhaust (~900 °C), leading to severe sintering of precious metal particles. Because this decreases their catalytic activity, greater quantities of precious metals are needed to maintain the high performance of TWCs. Consequently, one way to decrease the use of precious metals is to inhibit the sintering of precious metals. Recently, Nagai et al. [10] reported that Pt in Pt/ceria-based oxide does not sinter after aging treatment at 800 °C in air but does sinter in Pt/Al_2O_3. This phenomenon was explained by the formation of Pt–O–Ce bonds (i.e., the Pt-oxide–support interaction), which act as an anchor for Pt particles on ceria-based oxides.

Improving the intrinsic performance of TWCs is the most important approach to developing highly active catalysts with low precious metal loading. Extensive research and development has been performed for this purpose; for example, the performance of TWCs has been improved by the addition of many kinds of promoters. Although numerous investigations have been carried out to elucidate the effect of promoters, areas requiring study remain.

The latest generation of TWCs uses $CeO_2–ZrO_2$ materials. Incorporation of ZrO_2 into the CeO_2 lattice can improve both the thermal stability and the reducibility of metal-loaded $CeO_2–ZrO_2$ oxides [11,12]. In addition, the formation of $CeO_2–ZrO_2$ solid solutions causes different surface properties depending on the Ce/Zr composition [13]. These observations suggest that the use of $CeO_2–ZrO_2$ solid solutions with different compositions as a support

* Corresponding author. Fax: +81 29 861 4647.
E-mail address: m.haneda@aist.go.jp (M. Haneda).

0021-9517/$ – see front matter
doi:10.1016/j.jcat.2008.08.007

strongly influences the catalytic performance of the supported precious metals. In the present study, we prepared rhodium supported on CeO_2–ZrO_2 mixed oxides with different Ce/Zr compositions and measured the catalytic activity for NO reduction with C_3H_6 under stoichiometric conditions, to investigate the influence of Ce/Zr composition on catalytic activity in depth. We chose rhodium because of its high NO conversion rate [14]. We also performed catalyst characterizations as well as in situ FT-IR studies to investigate the possible factors directly affecting the catalytic performance of Rh/CeO_2–ZrO_2 catalysts.

2. Experimental

2.1. Catalyst preparation

CeO_2–ZrO_2 mixed oxides with different molar compositions were prepared using a coprecipitation method, in which a precipitate was produced by mixing a precipitant and an aqueous solution of cerium(III) nitrate and zirconium(IV) dinitrate oxide. The precipitant was a mixed solution of NH_4OH and $(NH_4)_2CO_3$. The precipitate thus obtained was washed with distilled water, dried, and calcined at 600 °C for 5 h in air. Hereinafter, CeO_2–ZrO_2 is referred to as CZ-X/Y, with X and Y representing the molar percentage of CeO_2 and ZrO_2, respectively.

The deposition of rhodium onto CeO_2–ZrO_2 was carried out by impregnation using a solution of rhodium(III) nitrate. The catalyst precursor was finally calcined at 600 °C for 5 h in air. The loading of rhodium was fixed at 0.4 wt%.

2.2. Catalytic activity measurement

Catalytic activity was evaluated using a fixed-bed continuous-flow reactor. A 0.1 g catalyst sample was held in a quartz tube (10 mm i.d.) by packing quartz wool at both ends of the catalyst bed. Before each reaction, the catalyst was pretreated in situ in the flow of reaction gas at 600 °C for 0.5 h. The reaction gas was a stoichiometric mixture of 500 ppm NO, 1167 ppm C_3H_6, 0.5% O_2, 10% H_2O, and the balance N_2. In some experiments, either NO or O_2 was removed from the reaction gas while keeping the concentrations of the other gases constant. The flow rate of the reaction gas was 1000 $cm^3\,min^{-1}$, which corresponds to 500,000 h^{-1} in GHSV. The catalytic activity was measured while the temperature was raised from 100 to 600 °C at a rate of 10 °C min^{-1}. The concentrations of NO_x, O_2, CO, and CO_2 in the effluent gas were continuously monitored using an online gas analyzer (Horiba, PG-240).

2.3. Catalyst characterization

The crystal structure was identified by XRD (Mac Science M18XHF^{22}) measurements using Cu$K\alpha$ radiation at 40 kV and 150 mA. The BET surface area of the samples was determined using a volumetric adsorption apparatus (Quantachrome, Nova-4200e) by N_2 adsorption at −196 °C.

The amount of chemisorbed CO was measured using a pulse method. The sample (50 mg) was first reduced with H_2 at 400 °C for 1 h, then cooled to 50 °C in flowing He. The sample was then treated consecutively with O_2, CO_2, and H_2 to poison the surface of the CeO_2 with CO_2 but to maintain the reducing state of Rh, because CeO_2 adsorbs CO as CO_2, leading to large errors in the chemisorption values [15]. Several pulses of CO were introduced to the sample until adsorption was no longer observed.

Temperature-programmed reduction (TPR) measurements were carried out to estimate the reducibility of the Rh/CeO_2–ZrO_2 catalysts. Each catalyst sample (100 mg) was oxidized with 20% O_2/N_2 at 600 °C for 1 h and cooled to room temperature. The gas flow was then switched to 10% H_2/Ar, and the temperature was raised to 920 °C at a rate of 10 °C min^{-1}. The consumption of H_2 was monitored using a thermal conductivity detector (TCD).

2.4. FT-IR study

2.4.1. CO adsorption measurement

A self-supporting sample disk, about 15 mg cm^{-2}, was placed in an IR cell with CaF_2 windows and pretreated in a flow of 10% H_2/He at 400 °C and subsequently cooled to 50 °C in flowing He. The activated sample disk was exposed to 0.5% CO/He flowing gas at 50 °C for 1 h, and then purged with He. IR spectra were recorded at 50 °C using a Nicolet Nexus 670 FT-IR spectrometer, accumulating 64 scans at a resolution of 4 cm^{-1}.

2.4.2. In situ diffuse reflectance FT-IR measurement

The diffuse reflectance FT-IR spectra were recorded with a Nicolet Nexus 670 FT-IR spectrometer, accumulating 64 scans at a resolution of 4 cm^{-1}. Before each experiment, 50 mg of a catalyst placed in a diffuse reflectance high temperature cell (Spectra Tech), fitted with CaF_2 windows, was pretreated in a flow of reaction gas containing 500 ppm NO, 1167 ppm C_3H_6, 0.5% O_2, and the balance He at 600 °C, and then cooled to the desired temperature in He. The background spectrum of the surface thus treated was measured for spectral correction. Observation of surface species was carried out after introducing a reaction gas containing one or more gas components comprising 500 ppm NO, 1167 ppm C_3H_6, 0.5% O_2, and the balance He at a flow rate of 30 $cm^3\,min^{-1}$.

3. Results

3.1. Physical properties of the catalysts

Because a mixture of CeO_2 and ZrO_2 is known to form a solid solution, the crystallite structure of the CeO_2–ZrO_2 samples was analyzed. Fig. 1 shows the XRD patterns of the Rh/CeO_2–ZrO_2 samples. No differences in the XRD patterns between the CeO_2–ZrO_2 and Rh/CeO_2–ZrO_2 samples were found. CeO_2 was found to have a fluorite-type structure; ZrO_2, a monoclinic-type structure. Clearly, only diffraction peaks attributable to the fluorite-type structure were observed for the four CeO_2–ZrO_2 samples, and each peak shifted to a higher angle with increasing ZrO_2 content, indicating formation of solid solutions of CeO_2 and ZrO_2. Some asymmetric peaks were observed in the XRD patterns, suggesting a partial segregation of different phases. No XRD peaks ascribed to rhodium

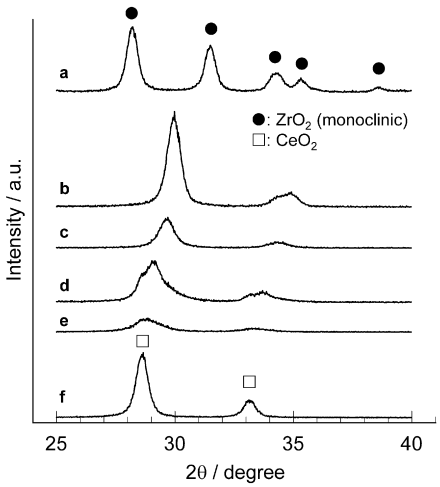

Fig. 1. XRD patterns of (a) Rh/CZ-0/100, (b) Rh/CZ-15/85, (c) Rh/CZ-32/68, (d) Rh/CZ-50/50, (e) Rh/CZ-74/26 and (f) Rh/CZ-100/0.

Table 1
Physical properties of the prepared $Rh/CeO_2–ZrO_2$

	Composition (mol%)		BET surface area ($m^2\,g^{-1}$)	Crystallite size[a] (nm)	Rh dispersion (CO/Rh)
	CeO_2	ZrO_2			
Rh/CZ-0/100	0	100	47	n.a.	0.32
Rh/CZ-15/85	15	85	61	12.7	0.44
Rh/CZ-32/68	32	68	59	11.9	0.77
Rh/CZ-50/50	50	50	81	7.90	0.23
Rh/CZ-74/26	74	26	77	6.74	0.48
Rh/CZ-100/0	100	0	63	13.6	0.67

[a] The crystallite size of $CeO_2–ZrO_2$ solid solution was calculated from the X-ray diffraction peak given in Fig. 1, from the (111) plane (2θ = ca. 28.6°) using Scherrer's equation.

species were seen in any of the samples, likely due to its low loading (0.4 wt%).

Table 1 summarizes the physical properties of $Rh/CeO_2–ZrO_2$ prepared in this study. The BET surface area was increased by mixing CeO_2 and ZrO_2 and reached a maximum value for CZ-50/50. Impregnation of Rh into $CeO_2–ZrO_2$ did not cause major changes in the BET surface area. A good correlation was observed between the BET surface area and the crystallite size of $CeO_2–ZrO_2$ solid solution calculated from the X-ray diffraction peak, given in Fig. 1, due to the (111) plane (2θ = ca. 28.6°) using Scherrer's equation. The samples with high surface area, CZ-50/50 and CZ-74/26, had small crystallites.

As Table 1 shows, Rh dispersion, estimated from CO chemisorption by assuming a stoichiometry of 1.0 CO/Rh [16], differed greatly according to the Ce/Zr molar ratio. Rh supported on CZ-32/68 and CZ-100/0 was highly dispersed, whereas Rh on CZ-50/50 had low dispersion. No clear relationship between Rh dispersion and BET surface area was seen.

3.2. Catalytic activity of $Rh/CeO_2–ZrO_2$

3.2.1. $NO + C_3H_6 + O_2$ reaction

Fig. 2 shows the NO and C_3H_6 conversion as a function of temperature for the NO + C_3H_6 + O_2 reaction over the $Rh/CeO_2–ZrO_2$ catalysts. The activity for NO reduction, as seen in Fig. 2A, was dependent on catalyst composition. The value of T_{50} for NO (the temperature giving NO conversion of 50%) over Rh/ZrO_2 was shifted to a lower temperature by mixing with CeO_2, indicating that the use of $CeO_2–ZrO_2$ as support effectively allowed NO reduction to proceed. The minimum value of T_{50} for NO (meaning the highest activity) was obtained on Rh/CZ-50/50. In contrast, further increases in CeO_2 content caused a sharp increase in T_{50}. Rh/CZ-74/26 and Rh/CZ-100/0 gave similar activity for NO reduction.

In accordance with the results for NO conversion, C_3H_6 conversion over $Rh/CeO_2–ZrO_2$ increased with increasing CeO_2 content up to 50 mol%, as shown in Fig. 2B; however, the use of $CeO_2–ZrO_2$ support with a high CeO_2 content (CZ-74/26) gave a minimum activity for C_3H_6 oxidation. Interestingly, in contrast, Rh/CeO_2 exhibited the greatest activity for C_3H_6 oxidation at very low NO reduction activity. Thus, Rh/CeO_2 appears to be a selective catalyst for C_3H_6 oxidation by O_2.

3.2.2. Unit reactions in the $NO + C_3H_6 + O_2$ reaction

3.2.2.1. $NO + C_3H_6$ reaction Fig. 3 compares the catalytic activity of Rh/CZ–50/50 and Rh/CZ-74/26 (which exhibited the best and worst activity for the NO + C_3H_6 + O_2 reaction, respectively) for NO reduction in the NO–C_3H_6 and NO–C_3H_6–O_2 reaction systems. Clearly, the light-off temperature for both catalysts was lower in the absence of O_2, suggesting that O_2 inhibited NO reduction with C_3H_6. Notably, a significant retarding effect of O_2 was observed for the Rh/CZ-74/26 catalyst (Fig. 3B).

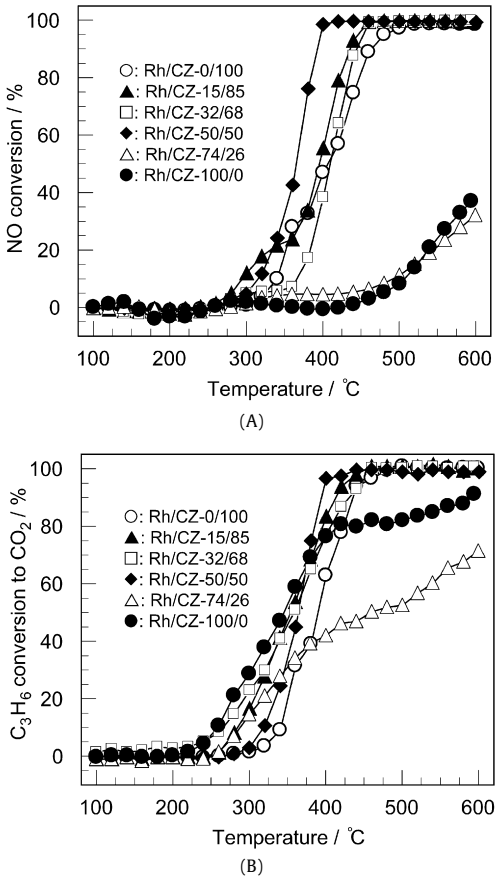

Fig. 2. (A) NO conversion and (B) C_3H_6 conversion to CO_2 vs. temperature for NO + C_3H_6 + O_2 reaction under stoichiometric conditions over $Rh/CeO_2–ZrO_2$ catalysts. (○) Rh/CZ-0/100, (▲) Rh/CZ-15/85, (□) Rh/CZ-32/68, (◆) Rh/CZ-50/50, (△) Rh/CZ-74/26 and (●) Rh/CZ-100/0. Reaction conditions: NO 500 ppm, O_2 0.5%, C_3H_6 1167 ppm, H_2O 10%, N_2 balance, catalyst weight = 0.1 g, total flow rate = 1000 $cm^3\,min^{-1}$, heating rate = 10 °C min^{-1}.

3.2.2.2. $C_3H_6 + O_2$ reaction Fig. 4 shows the activity of C_3H_6 oxidation in the reaction system of NO–C_3H_6–O_2 and C_3H_6–O_2 over Rh/CZ-50/50 and Rh/CZ-74/26 catalysts. As can be seen in Fig. 4A, C_3H_6 oxidation over Rh/CZ-50/50 was inhibited by the presence of NO, suggesting that Rh/CZ-50/50 has high C_3H_6 utilization for NO reduction. On the other hand, no difference in C_3H_6 conversion was observed for the NO + C_3H_6 + O_2 and C_3H_6 + O_2 reactions over Rh/CZ-74/26 (Fig. 4B). This indicates that C_3H_6 oxidation by O_2 occurs preferentially in the NO + C_3H_6 + O_2 reaction over the Rh/CZ-74/26 catalyst.

3.2.3. Response of activity to O_2 addition for $NO + C_3H_6$ reaction over Rh/CZ-74/26

To gain insight into the inhibiting effect of O_2 for NO reduction over Rh/CZ-74/26, the response of NO and C_3H_6 conversions to an intermittent feed of 0.5% O_2 was measured at 350 °C. The NO + C_3H_6 reaction was started from 100 to 350 °C at a heating rate of 10 °C min^{-1}, after which the introduction and removal of O_2 was carried out at 350 °C. The results are given in Fig. 5.

During the reaction in the absence of O_2, NO conversion reached 85%, but when O_2 was added to the reaction gas, NO conversion quickly fell to 5%. Removal of O_2 from the reaction gas caused an increase in NO conversion to the initial value. The same phenomenon was observed for C_3H_6 conversion to CO_2, although the presence of O_2 showed the opposite effect. Specifically, C_3H_6 conversion was increased by the addition of O_2. These findings indicate that the effect of O_2 is reversible.

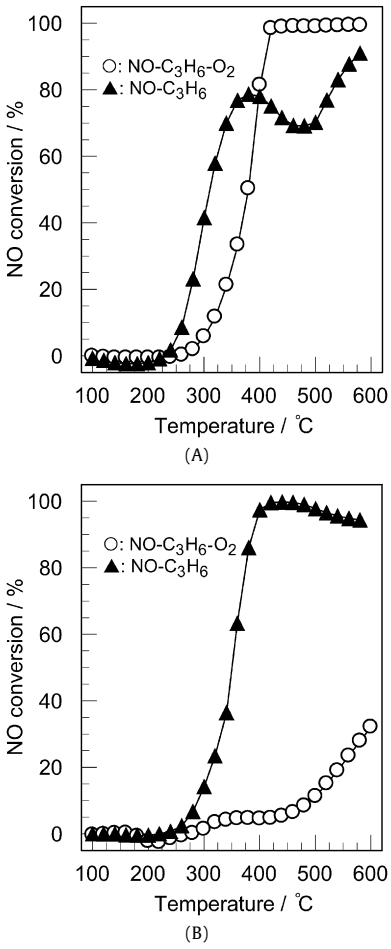

Fig. 3. Comparison of NO conversion over (A) Rh/CZ-50/50 and (B) Rh/CZ-74/26 for NO + C_3H_6 + O_2 (○) and NO + C_3H_6 reactions (▲). Reaction conditions: NO 500 ppm, O_2 0 or 0.5%, C_3H_6 1167 ppm, H_2O 10%, N_2 balance, catalyst weight 0.1 g, total flow rate 1000 $cm^3\,min^{-1}$, heating rate 10 °C min^{-1}.

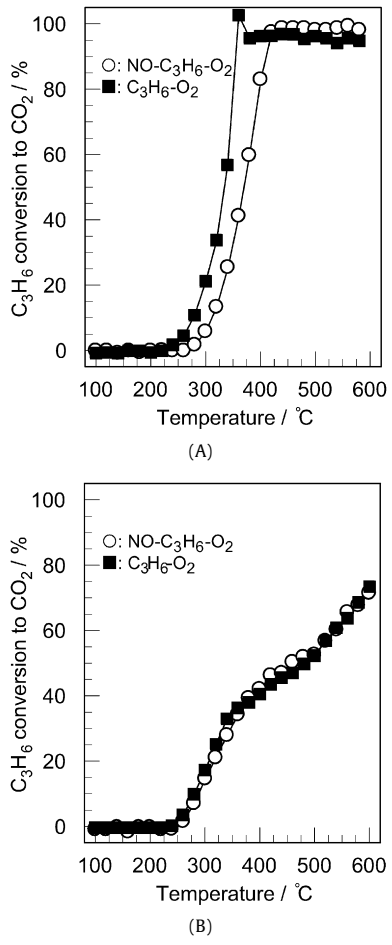

Fig. 4. Comparison of C_3H_6 conversion to CO_2 over (A) Rh/CZ-50/50 and (B) Rh/CZ-74/26 for NO + C_3H_6 + O_2 (○) and C_3H_6 + O_2 reactions (■). Reaction conditions: NO 0 or 500 ppm, O_2 0.5%, C_3H_6 1167 ppm, H_2O 10%, N_2 balance, catalyst weight = 0.1 g, total flow rate = 1000 $cm^3\,min^{-1}$, heating rate = 10 °C min^{-1}.

3.3. Reduction behavior of Rh/CeO_2–ZrO_2 by TPR

Fig. 6 shows TPR profiles of CeO_2–ZrO_2 as catalyst support. The TPR profile of CeO_2 (CZ-100/0) showed two reduction peaks at around 300–580 °C and 815 °C. These can be attributed to the successive reduction of the surface and bulk of CeO_2, respectively [2]. For CeO_2–ZrO_2 mixed oxides, one strong reduction peak appeared in their TPR profiles with a maximum at 530–590 °C. Among the CeO_2–ZrO_2 catalysts evaluated, the CZ-50/50 gave a very sharp peak, suggesting the quite fast reduction of CeO_2–ZrO_2.

Fig. 7 shows the TPR profiles of Rh/CeO_2–ZrO_2 samples. Obviously, the H_2 consumption peaks were shifted to lower temperature by presence of Rh, suggesting that Rh promotes the reduction of CeO_2–ZrO_2, as reported previously [17]. As can be seen in Fig. 7, all of the samples except Rh/CZ-50/50 gave a reduction peak at around 100 °C. These peaks may be ascribed to the reduction of rhodium oxide and cerium oxide. But the H_2 uptake for the reduction of rhodium oxide was low compared with that for CeO_2, because the loading of rhodium was 0.4 wt%. Quantitative comparison of TPR peaks observed for CeO_2–ZrO_2 and Rh/CeO_2–ZrO_2 also suggests that the amount of H_2 uptake observed for Rh/CeO_2–ZrO_2 was slightly smaller than that for the reduction of CeO_2–ZrO_2 support. Consequently, the reduction peak at around 100 °C can be ascribed mainly to the reduction of the vicinity of the CeO_2–ZrO_2, which is strongly interacting with rhodium.

In the TPR profile of the Rh/CZ-50/50 sample, two broad reduction peaks were observed in the region of 120–300 °C and 400–550 °C. Because the total H_2 uptake was similar to that for the reduction of the CZ-50/50 support, these two peaks can be attributed to the successive reduction of the vicinity of the CeO_2–ZrO_2 support interacting with rhodium and then the bulk CeO_2–ZrO_2 support.

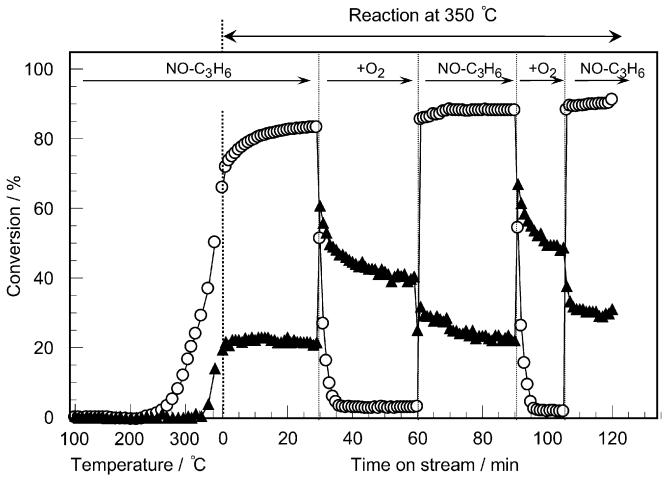

Fig. 5. Response of NO conversion (○) and C_3H_6 conversion to CO_2 (▲) to intermittent feed of O_2 over Rh/CZ-74/26 at 350 °C for NO reduction with C_3H_6. Reaction conditions: NO 500 ppm, O_2 0 or 0.5%, C_3H_6 1167 ppm, H_2O 10%, N_2 balance, catalyst weight = 0.1 g, total flow rate = 1000 $cm^3\,min^{-1}$.

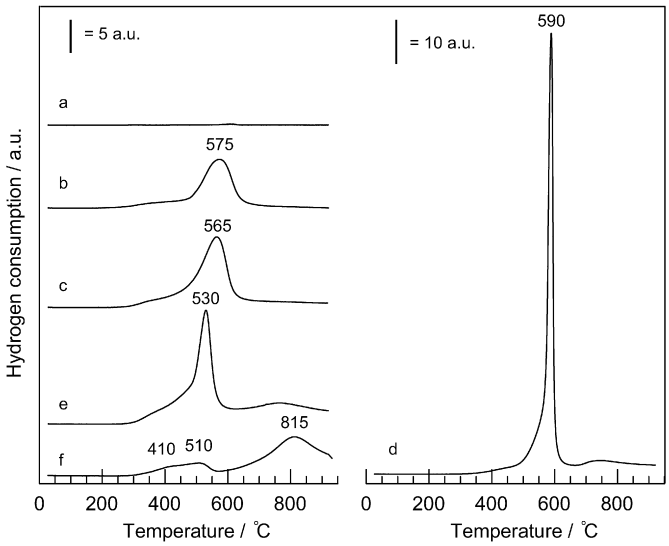

Fig. 6. TPR profiles of (a) CZ-0/100, (b) CZ-15/85, (c) CZ-32/68, (d) CZ-50/50, (e) CZ-74/26 and (f) CZ-100/0.

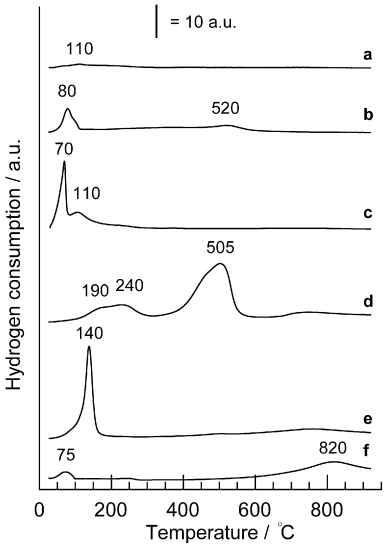

Fig. 7. TPR profiles of (a) Rh/CZ-0/100, (b) Rh/CZ-15/85, (c) Rh/CZ-32/68, (d) Rh/CZ-50/50, (e) Rh/CZ-74/26 and (f) Rh/CZ-100/0.

3.4. Study of rhodium surface by FT-IR after CO adsorption

The interaction between CO and supported Rh is known to produce three distinct adsorption modes—dicarbonyl, linear-bonded CO, and bridged-bonded CO—depending on the particle size and oxidation state of Rh [18,19]. To investigate the oxidation state of Rh surface, FT-IR spectra of CO species as a probe molecule adsorbed on the Rh/CeO_2–ZrO_2 were measured.

As shown in Fig. 8, exposure of CO to Rh/CeO_2–ZrO_2 gave IR bands in the region above 2000 cm^{-1} due to adsorption of the CO species on Rh. Similar FT-IR spectra were clearly seen for Rh/CZ-0/100, Rh/CZ-15/85, Rh/CZ-32/68, and Rh/CZ-74/26. Sets of bands assignable to the asymmetric and symmetric stretching vibrations of a gem-dicarbonyl species on Rh^+ ($Rh^+(CO)_2$) [20–23] were detected at ca. 2087 and 2015 cm^{-1}, respectively. In the case of Rh/CZ-74/26 (spectrum e) only, a weak band assignable to CO species linearly bonded on Rh^+ (Rh^+–CO) [21,22] or Rh^0 (Rh^0–CO) [19,23–25] appeared at 2052 cm^{-1}.

In contrast, for Rh/CZ-100/0 (Rh/CeO_2), two sets of bands were seen at 2089 and 2023 cm^{-1} and 2073 and 2005 cm^{-1}, assigned to gem-dicarbonyl species, suggesting the presence of two different Rh^+ sites. In addition to these bands, a strong band assignable to CO species linearly bonded on Rh^{2+} [19,26] appeared at 2100 cm^{-1}. The band at 2110 cm^{-1} may be assigned to linearly bonded CO on Rh^{3+}, according to a previous study in which similar IR bands were observed for Rh/TiO_2 [19]. The formation of Rh species with a higher oxidation state seems to be favored on the CeO_2 surface, in agreement with a previous report [27].

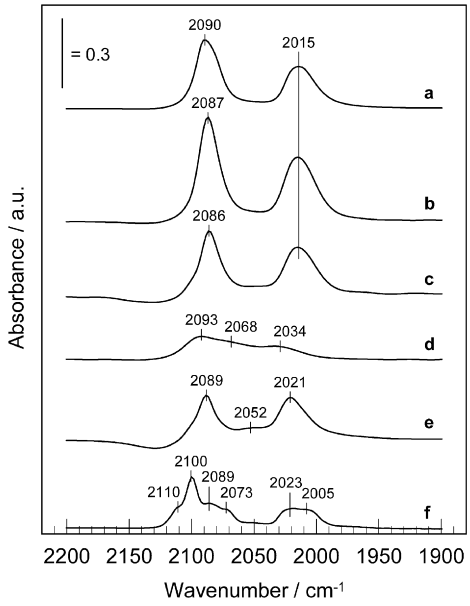

Fig. 8. FT-IR spectra of CO adsorbed onto (a) Rh/CZ-0/100, (b) Rh/CZ-15/85, (c) Rh/CZ-32/68, (d) Rh/CZ-50/50, (e) Rh/CZ-74/26 and (f) Rh/CZ-100/0. All the spectra were recorded after flushing with He at 50 °C following exposure to 0.5% CO/He at 50 °C for 1 h.

As can be seen in Fig. 8, two broad IR bands at 2093 and 2034 cm^{-1} and a shoulder band at 2068 cm^{-1} due to either Rh^+–CO or Rh^0–CO were present in the spectrum for Rh/CZ-50/50. Although the former two bands can be assigned to $Rh^+(CO)_2$, the $\Delta\nu$(C=O) shift between the symmetric and asymmetric stretching mode of the gem-dicarbonyl species for Rh/CZ-50/50 (59 cm^{-1}) differs from that for the other catalysts (70–75 cm^{-1}). A wide variety of $\Delta\nu$(C=O) shifts between 60 and 75 cm^{-1}, related to the type of support and Rh dispersion, have been reported previously [19,20,22–24,27–29], suggesting that the surface properties of Rh, such as electron density and site geometry, are different in Rh/CZ-50/50 than in the other catalysts.

3.5. Observation of surface species by in situ diffuse reflectance FT-IR spectroscopy

3.5.1. Steady-state reaction

Figs. 9 and 10 show the IR spectra recorded during the NO + C_3H_6 + O_2 reaction over Rh/CZ-50/50 and Rh/CZ-74/26 catalysts, respectively, in the temperature range 250–500 °C. Very similar IR spectra were observed for both catalysts—namely, the IR bands due to carboxylate species at around 1430–1550 cm^{-1} [30] and due to formate species at 1360 and 1371 cm^{-1} [31] were detected. The IR bands in the region of 2700–3000 cm^{-1} appear to be assigned to the ν(CH) vibration mode and the overtone due to $\nu_{as}(COO^-)$ + δ(CH) modes of adsorbed formate species [31,32]. Relevant band assignments are listed in Table 2. The intensity of these bands decreased with increasing reaction temperature. It should be noted that the carboxylate and formate species were still observed on Rh/CZ-74/26 at 500 °C, whereas only carboxylate species with very weak band was observed on Rh/CZ-50/50 at 450 °C, suggesting

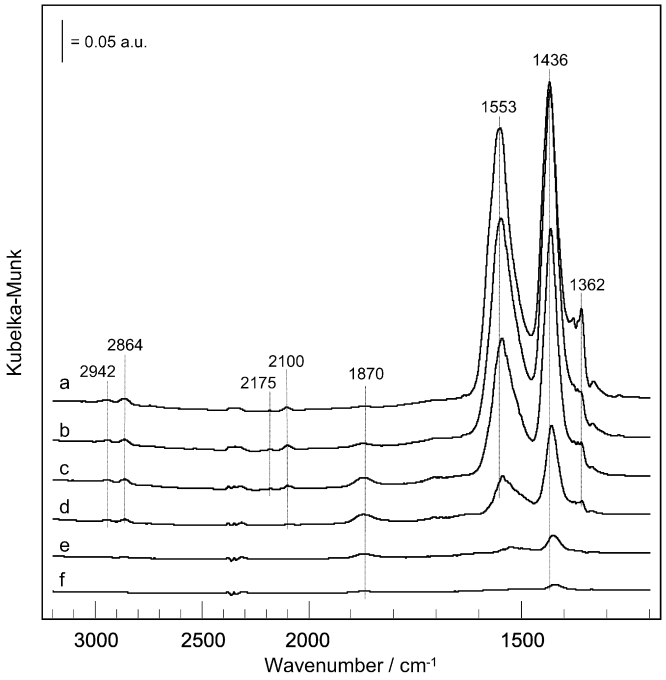

Fig. 9. Diffuse reflectance FT-IR spectra of adsorbed species formed during the NO + C_3H_6 + O_2 reaction over Rh/CZ-50/50 at (a) 250, (b) 300, (c) 350, (d) 400, (e) 450 and (f) 500 °C for 30 min. Conditions: NO 500 ppm, O_2 0.5%, C_3H_6 1167 ppm, He balance, catalyst weight = 50 mg, total flow rate = 30 $cm^3\,min^{-1}$.

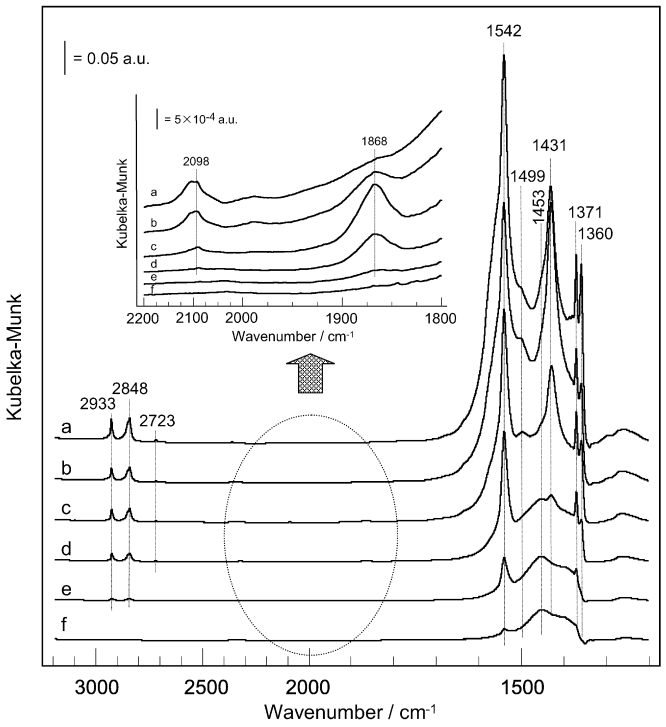

Fig. 10. Diffuse reflectance FT-IR spectra of adsorbed species formed during the NO + C_3H_6 + O_2 reaction over Rh/CZ-74/26 at (a) 250, (b) 300, (c) 350, (d) 400, (e) 450 and (f) 500 °C for 30 min. Conditions: NO 500 ppm, O_2 0.5%, C_3H_6 1167 ppm, He balance, catalyst weight = 50 mg, total flow rate = 30 $cm^3\,min^{-1}$.

Table 2
Wavenumber and assignments of absorption bands in FT-IR spectra

Wavenumber (cm^{-1})	Surface species	Vibration	References
1553	Carboxylate COO^-	ν_{as}(OCO)	[30]
1436		ν_s(OCO)	
2931	Formate $HCOO^-$	ν_{as}(OCO) + δ(CH)	[31,32]
2847		ν(CH)	
1371		δ(CH)	
1360		ν_s(OCO)	
2100	CO–Rh^{2+}		[19–26]
2062	gem-dicarbonyl ($Rh^+(CO)_2$)		
2000			
1870	NO–$Rh^{\delta+}$	ν(NO)	[33]
2175	Cyanide –CN		[21]

that Rh/CZ-74/26 can strongly adsorb the carboxylate and formate species.

In addition to the bands due to carboxylate and formate species, weak but distinct IR bands at 1870, 2100, and 2175 cm^{-1} assignable to positively charged NO species adsorbed onto Rh ($Rh(NO)^{\delta+}$) [33], CO species linearly adsorbed onto Rh^{2+} [19,26] and CN species adsorbed onto Rh species [21], respectively, appeared in the IR spectra for Rh/CZ-50/50 (Fig. 9). The bands due to Rh^{2+}(CO) and Rh–CN species decreased with increasing temperature and disappeared completely at 400 °C. It also is noteworthy that $Rh(NO)^{\delta+}$ increased with reaction temperature, reaching a maximum at 400 °C and then decreasing. As can be seen in Fig. 10, the IR band due to $Rh(NO)^{\delta+}$ at 1868 cm^{-1} was observed for Rh/CZ-74/26 as well. But its band intensity was quite weak compared with that of Rh/CZ-50/50 likely because the formation of carboxylate and formate species was favorable on the surface of Rh/CZ-74/26, resulting in insufficient reaction sites for NO reduction.

3.5.2. Transient reactions

The low catalytic performance of Rh/CZ-74/26 for NO reduction by C_3H_6 is assumed to be related to the formation of carboxylate and formate species. But NO reduction by C_3H_6 occurred over Rh/CZ-74/26 in the absence of O_2 (Fig. 3B), and a good response of activity to O_2 addition and its removal was observed (Fig. 5). A transient response study of the IR spectra was carried out to investigate the contribution of O_2 to the behavior of surface species for the reaction system of NO–C_3H_6 and NO–C_3H_6–O_2 over Rh/CZ-74/26 at 350 °C. Fig. 11A shows the IR spectra obtained in the NO–C_3H_6 reaction system. Bands due to gem-dicarbonyl species ($Rh^+(CO)_2$) at 2062 and 2000 cm^{-1} and –CN species at 2167 cm^{-1} clearly appeared at the beginning of the reaction, and their intensity increased with reaction time. Carboxylate species, which give characteristic bands in the region of 1550–1400 cm^{-1}, also increased with reaction time. In contrast, formate species formed at the beginning of the reaction, then decreased with reaction time. This can be clearly seen in Fig. 12, which shows a change in the peak area of 2940–2832 cm^{-1} due to formate species as a function of reaction time. This finding suggests that formate species did not accumulate on the surface under reaction conditions when O_2 was not present.

When O_2 was introduced into the reaction gas, the gem-dicarbonyl species and –CN species were almost completely removed, as shown in Fig. 11B. Carboxylate species also were decreased slightly with increasing reaction time. On the other hand, the formate species (2931 and 2847 cm^{-1}) increased gradually with reaction time after the introduction of O_2, then reached a plateau (Fig. 12). When O_2 was again removed from the reaction gas, the formate species decreased rapidly. The behavior of formate species toward O_2 ON/OFF is in good agreement with that of NO conversion, shown in Fig. 5.

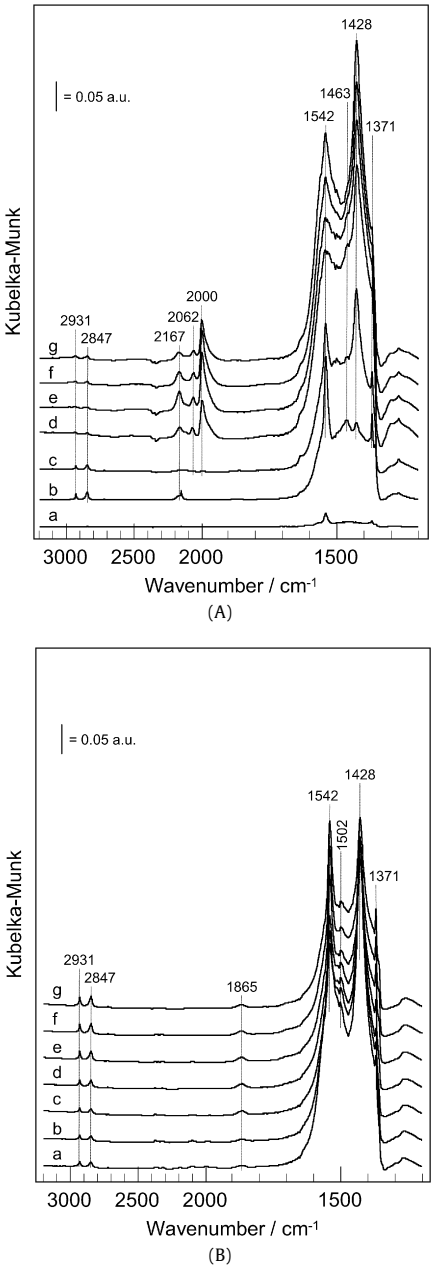

Fig. 11. Diffuse reflectance FT-IR spectra of adsorbed species formed during (A) the NO + C_3H_6 reaction and (B) the NO + C_3H_6 + O_2 reaction following introduction of 0.5% O_2 into the reaction gas of NO–C_3H_6/He over Rh/CZ-74/26 at 350 °C for (a) 0.5, (b) 1.5, (c) 5, (d) 10, (e) 15, (f) 20 and (g) 30 min. Conditions: NO 500 ppm, O_2 0 or 0.5%, C_3H_6 1167 ppm, He balance, catalyst weight = 50 mg, total flow rate = 30 $cm^3\,min^{-1}$.

4. Discussion

4.1. Influence of rhodium/CeO_2–ZrO_2 support interaction

The catalytic activity of Rh/CeO_2–ZrO_2 for NO reduction by C_3H_6 under stoichiometric conditions depends strongly on the Ce/Zr composition (Fig. 2). Rh/CeO_2–ZrO_2 with a Ce/Zr molar ratio of 50/50 (Rh/CZ-50/50) exhibited the most activity; Rh/CZ-74/26, the least. As summarized in Table 1, no significant differences in the bulk properties, such as BET surface area or crystallite size of the CeO_2–ZrO_2 support, were observed for Rh/CZ-50/50 and Rh/CZ-74/26, suggesting that the bulk properties of CeO_2–ZrO_2 did not directly contribute to catalytic performance.

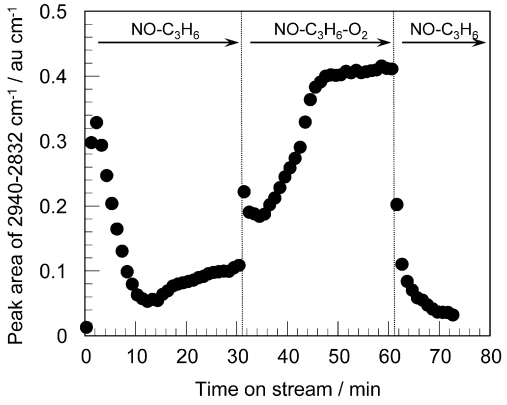

Fig. 12. Time-dependence of the integrated area of the bands due to formate species in the region of 2940–2832 cm^{-1} formed during the NO + C_3H_6 reaction over Rh/CZ-74/26 at 350 °C, when O_2 was introduced into and removed from the reaction gas. Conditions: NO 500 ppm, O_2 0 or 0.5%, C_3H_6 1167 ppm, He balance, catalyst weight = 50 mg, total flow rate = 30 $cm^3\,min^{-1}$.

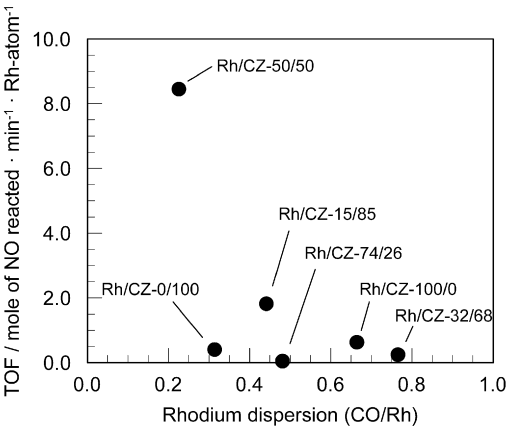

Fig. 13. Turnover frequency (TOF) for NO reduction into N_2 in the NO–C_3H_6–O_2 reaction system over Rh/CeO_2–ZrO_2 at 360 °C as a function of Rh dispersion.

Because we confirmed in a separate experiment that the activity of the CeO_2–ZrO_2 support was quite low, the active species of the Rh/CeO_2–ZrO_2 catalyst for NO + C_3H_6 + O_2 reaction must have been Rh. If the CeO_2–ZrO_2 support does not affect the catalytic performance of Rh, then the activity of Rh/CeO_2–ZrO_2 should be explained by the Rh dispersion. To clarify this point, TOF (expressed as moles of NO reduced to N_2 per mole of surface Rh atoms per minute) was calculated, with the reaction rate for NO reduction to N_2 measured under nearly differential reaction conditions giving NO conversion <20% by varying the catalyst weight. Fig. 13 shows the change in TOF at 360 °C as a function of Rh dispersion. Interestingly, a quite high TOF was obtained for Rh/CZ-50/50, with the lowest Rh dispersion (CO/Rh = 0.23); however, a slight increase in Rh dispersion (0.23 → 0.32) caused a sharp drop in the TOF. Above 30% Rh dispersion, no clear relationship between the TOF and Rh dispersion was observed. This finding suggests that the catalytic performance of Rh/CeO_2–ZrO_2 cannot be explained simply by Rh dispersion; therefore, the CeO_2–ZrO_2 support seems to affect the catalytic performance of Rh.

The surface properties of Rh, responsible for the catalytic performance, depend strongly on the interaction with the CeO_2–ZrO_2 support. The difference in the reducibility of Rh and CeO_2–ZrO_2 demonstrated by TPR measurements provides information on the Rh and CeO_2–ZrO_2 support interaction. As can be seen in Fig. 7, the reduction peak of the CeO_2–ZrO_2 support interacting with Rh appeared at different temperatures according to the Ce/Zr composition. The reducibility of noble metals is known to be affected

significantly by the metal–support interaction [2]. The reduction of supported noble metals is generally more difficult than that of unsupported ones [34]. Therefore, the presence of H_2 uptake peak at lower temperatures suggests the presence of weak Rh and CeO_2–ZrO_2 support interaction. Taking this concept into account, the Rh and CeO_2–ZrO_2 support interaction seems to increase in the following order: Rh/CZ-100/0 ≈ Rh/CZ-32/68 < Rh/CZ-15/85 < Rh/CZ-74/26 ≪ Rh/CZ-50/50.

Because catalytic reactions occur on the catalyst surface, the electron density and site geometry of Rh surface, which are affected by the Rh and CeO_2–ZrO_2 support interaction, are important factors. As demonstrated by the FT-IR spectra of adsorbed CO species shown in Fig. 8, the gem-dicarbonyl species on Rh^+ ($Rh^+(CO)_2$) was predominantly detected for all of the samples; however, for Rh/CZ-50/50, the $\Delta\nu$(C=O) shift between the symmetric and asymmetric stretching mode of the gem-dicarbonyl species (59 cm^{-1}) differed from that for the other catalysts (70–75 cm^{-1}), suggesting a different site geometry of the Rh surface. Formation of the gem-dicarbonyl species ($Rh^+(CO)_2$) was interpreted by the oxidative disruption of Rh_x crystallites with the aid of surface OH groups on the support oxides [20,35–37], leading to the creation of oxidic Rh_x crystallites. The resulting oxidic Rh_x crystallites were stabilized on the surface of CeO_2–ZrO_2 support. Consequently, the unique surface properties of Rh species on CZ-50/50 can be ascribed to the strong interaction with the CeO_2–ZrO_2 support.

The order of the Rh and CeO_2–ZrO_2 support interaction was not exactly the same as the order of TOF; however, the Rh/CZ-50/50 with the highest TOF for NO reduction exhibited the strongest Rh and CeO_2–ZrO_2 support interaction. It can be concluded that the Rh and CeO_2–ZrO_2 support interaction is one of the important factors directly affecting the catalytic performance of Rh/CeO_2–ZrO_2 catalysts.

4.2. Influence of surface species formed during the reaction

As mentioned above, the specifically high activity of Rh/CZ-50/50 was attributed to the strong Rh and CeO_2–ZrO_2 support interaction. However, Rh/CZ-74/26, which showed no significant differences in the surface properties of Rh was the least active catalyst. Accordingly, some important factors other than the metal–support interaction must affect the catalytic performance.

Recall that Rh/CZ-74/26 was found to effectively catalyze NO reduction with C_3H_6 in the absence of O_2 (Fig. 3B), whereas its activity was very low in the presence of O_2 (Fig. 2). In the experiments evaluating the transient response of the activity to the intermittent feed of O_2 over Rh/CZ-74/26 (Fig. 5), an induction period to reach steady state was clearly observed when O_2 was added to the reaction gas. In contrast, no induction period was observed when O_2 was removed. These findings suggest that coexisting O_2 participates in the formation and/or decomposition of certain adsorbed species.

As shown in Figs. 9 and 10, many kinds of adsorbed species were formed during the NO + C_3H_6 + O_2 reaction over Rh/CZ-50/50 and Rh/CZ-74/26 at elevated temperatures. Carboxylate and formate species, positively charged NO species adsorbed onto Rh ($Rh(NO)^{\delta+}$), CO species linearly adsorbed onto Rh^{2+}, and CN species adsorbed onto Rh were detected as intermediate and/or spectator species. Among these, $Rh^{2+}(CO)$ and Rh–CN species were clearly seen in the IR spectra for Rh/CZ-50/50. Of interest, these two bands decreased with increasing temperature and disappeared completely at 400 °C, whereas the rate of NO reduction increased significantly (Fig. 2). These species may be intermediates in the NO + C_3H_6 + O_2 reaction over Rh/CZ-50/50.

According to Shelef and Graham [14], the initial elementary step in NO reduction over supported Rh catalysts in TWC applications is adsorption of NO onto the Rh surface. Exposure of NO to the Rh surface is known to lead to the formation of several types of NO species. Among these, the dinitrosyl species ($Rh(NO)_2$) has been proposed as a reaction intermediate [14,38], because only the dinitrosyl species was observed on supported Rh, which is favorable to the pairing of nitrogen. The participation of mononitrosyl species such as $Rh(NO)^{\delta-}$ and $Rh(NO)^{\delta+}$ in NO reduction by CO over supported Rh catalysts also has been reported [21,33].

In the present study, no formation of dinitrosyl species was observed, and only $Rh(NO)^{\delta+}$ was detected on Rh/CZ-50/50 (Fig. 9) and Rh/CZ-74/26 (Fig. 10), with more intense band for the former catalyst. $Rh(NO)^{\delta+}$ was found to increase with reaction temperature; to reach a maximum at 400 °C, at which the rate of NO reduction significantly increased (Fig. 2); and then to decrease. It also is noteworthy that the IR band due to $Rh(NO)^{\delta+}$ increased with decreasing concentration of carboxylate and formate species. The formation of $Rh(NO)^{\delta+}$ may have been a slow step at low temperatures, because the formation of carboxylate and formate species covering the reaction site was favorable. Because the reaction site appeared to be activated by desorbing carboxylate and formate species at high temperature, sufficient $Rh(NO)^{\delta+}$ was formed. The stability of carboxylate and formate species seemed to differ in the two catalysts, however. Carboxylate and formate species formed on the Rh/CZ-74/26 were more stable than those formed on the Rh/CZ-50/50; the carboxylate and formate species were still observed on Rh/CZ-74/26 at 500 °C, at which point NO reduction was initiated (Fig. 2). These results suggest that carboxylate and formate species poisoned the reaction sites for NO reduction.

Did carboxylate and formate species really poison the reaction sites? As described above, Rh/CZ-74/26 could effectively catalyze NO reduction with C_3H_6 in the absence of O_2 (Fig. 3B). If the aforementioned hypothesis were true, then the formation of carboxylate and formate species should not be prominent in the absence of O_2. As can be seen in Fig. 11A, the IR bands due to formate species at 2931 and 2847 cm^{-1} were very weak compared with those seen in the presence of O_2 (Fig. 10). Interestingly, formate species were formed at the beginning of the reaction and then decreased with increasing reaction time (Fig. 12). This finding suggests that formate species did not accumulate on the surface under reaction conditions in the absence of O_2. On the other hand, the formate species increased gradually with time after the introduction of O_2, and then reached a plateau (Fig. 12). When O_2 was removed again, the formate species decreased rapidly. The behavior of formate species toward O_2 ON/OFF is in good agreement with that of NO conversion, as shown in Fig. 5. Thus, it can be concluded that formate species poisoned the catalytically active sites for NO reduction with C_3H_6, resulting in the low NO reduction activity of Rh/CZ-74/26. Because no clear relationship between the formation of carboxylate species and the catalytic activity was found, carboxylate species did not poison the reaction sites.

5. Conclusion

In this study, the influence of Ce/Zr composition on the catalytic activity of Rh/CeO_2–ZrO_2 for NO reduction by C_3H_6 under stoichiometric conditions was investigated. The catalytic activity of Rh/CeO_2–ZrO_2 was found to be strongly dependent on the Ce/Zr composition. Among the catalysts tested here, Rh/CZ-50/50 showed the most activity, and Rh/CZ-74/26 the least. The Rh/CZ-50/50 catalyst also exhibited specifically high intrinsic activity expressed in terms of TOF. Physicochemical properties, such as BET surface area, Rh dispersion, reducibility measured by TPR, and the electron density of the Rh surface characterized by FT-IR after CO adsorption, varied according to the Ce/Zr composition and revealed differing Rh and CeO_2–ZrO_2 support interactions. The high TOF on Rh/CZ-

50/50 was accounted for by the strong Rh and CeO_2–ZrO_2 support interaction.

The activity of Rh/CeO_2–ZrO_2 for NO reduction by C_3H_6 also was found to depend strongly on the reaction gas conditions. Co-existing O_2 inhibited the NO reduction by C_3H_6, especially for the Rh/CZ-74/26. In situ FT-IR spectroscopy revealed that formate species, which were formed in significant amounts and stabilized on the Rh/CZ-74/26 catalyst, poisoned the catalytically active sites for NO reduction with C_3H_6.

References

[1] J.T. Kummer, Prog. Energy Combust. Sci. 6 (1979) 177.
[2] A. Trovarelli, Catal. Rev. Sci. Eng. 38 (1996) 439.
[3] R. Di Monte, J. Kašpar, Top. Catal. 28 (2004) 47.
[4] T. Miki, T. Ogawa, M. Haneda, N. Kakuta, A. Ueno, S. Tateishi, S. Matsuura, M. Sato, J. Phys. Chem. 94 (1990) 6464.
[5] M. Ozawa, M. Kimura, A. Isogai, J. Alloys Compd. 193 (1993) 73.
[6] T. Murota, T. Hasegawa, S. Aozasa, H. Matsui, M. Motoyama, J. Alloys Compd. 193 (1993) 298.
[7] A.D. Logan, M. Shelef, J. Mater. Res. 9 (1994) 468.
[8] Z.X. Song, W. Liu, H. Nishiguchi, A. Takami, K. Nagaoka, Y. Takita, Appl. Catal. A 329 (2007) 86.
[9] D. Jollie, Platinum 2007, Johnson Matthey, UK, 2006, p. 28.
[10] Y. Nagai, T. Hirabayashi, K. Dohmae, N. Takagi, T. Minami, H. Shinjoh, S. Matsumoto, J. Catal. 242 (2006) 103.
[11] P. Fornasiero, R. Di Monte, G.R. Rao, J. Kašper, S. Meriani, A. Trovarelli, M. Graziani, J. Catal. 151 (1995) 168.
[12] G. Balducci, J. Kašper, P. Fornasiero, M. Graziani, M. Siful Islam, J.D. Gale, J. Phys. Chem. B 101 (1997) 1750.
[13] M. Daturi, C. Binet, J.-C. Lavalley, A. Galtayries, R. Sporken, Phys. Chem. Chem. Phys. 1 (1999) 5717.
[14] M. Shelef, G.W. Graham, Catal. Rev.-Sci. Eng. 36 (1994) 433.
[15] T. Takeguchi, S. Manabe, R. Kikuchim, K. Eguchi, T. Kanazawa, S. Matsumoto, W. Ueda, Appl. Catal. A 293 (2005) 91.
[16] J. Oi, A. Obuchi, G.R. Bamwenda, A. Ogata, H. Yagita, S. Kushiyama, K. Mizuno, Appl. Catal. B 12 (1997) 277.
[17] G. Ranga Rao, P. Fornasiero, R. Di Monte, J. Kašper, G. Vlaic, G. Balducci, S. Meriani, G. Gubitosa, A. Cremona, M. Graziani, J. Catal. 162 (1996) 1.
[18] A.C. Yang, C.W. Garland, J. Phys. Chem. 61 (1957) 1504.
[19] S. Trautmann, M. Baerns, J. Catal. 150 (1994) 335.
[20] J. Raskó, J. Bontovics, Catal. Lett. 58 (1999) 27.
[21] D.I. Kondarides, T. Chafik, E. Verykios, J. Catal. 191 (2000) 147.
[22] K. Hadjiivanov, E. Ivanova, L. Dimitrov, H. Knözinger, J. Mol. Struct. 661–662 (2003) 459.
[23] G. Lafaye, C. Mihut, C. Especel, P. Marécot, M.D. Amiridis, Langmuir 20 (2004) 10612.
[24] C.A. Rice, S.D. Worley, C.W. Curtis, J.A. Guin, A.R. Tarrer, J. Phys. Chem. 74 (1981) 6487.
[25] G.N. Vayssilov, N. Rösch, J. Am. Chem. Soc. 124 (2002) 3783.
[26] J.P. Wey, W.C. Neely, S.D. Worley, J. Catal. 134 (1992) 378.
[27] T. Bánsági, T.S. Zakar, F. Solymosi, Appl. Catal. B 66 (2006) 147.
[28] E. Ivanova, M. Mihaylov, H.A. Aleksandrov, M. Daturi, F. Thibault-Starzyk, G.N. Vayssilov, N. Rösch, K.I. Hadjiivanov, J. Phys. Chem. C 111 (2007) 10412.
[29] Z.L. Zhang, A. Kladi, X.E. Verykios, J. Mol. Catal. 89 (1994) 229.
[30] A.A. Davydov, in: C.H. Rochester (Ed.), Infrared Spectroscopy of Adsorbed Species on the Surface of Transition Metal Oxides, Wiley, Chichester, 1990, p. 29.
[31] C. Chauvin, J. Saussey, J.C. Lavalley, H. Idriss, J. Hindermann, A. Kiennemann, P. Chaumette, P. Courty, J. Catal. 121 (1990) 56.
[32] E. Finocchio, M. Daturi, C. Binet, J.C. Lavalley, G. Blanchard, Catal. Today 52 (1999) 53.
[33] C. Dujardin, A.-S. Mamede, E. Payen, B. Sombret, J.P. Huvenne, P. Grangrer, Top. Catal. 30/31 (2004) 347.
[34] H.C. Yao, M. Sieg, H.K. Plummer, J. Catal. 59 (1979) 365.
[35] F. Solymosi, M. Pásztor, G. Rákhely, J. Catal. 110 (1988) 413.
[36] M.I. Zaki, T.H. Ballinger, J.T. Yates Jr., J. Phys. Chem. 95 (1991) 4028.
[37] T.T. Wong, A.Y. Stakheev, W.M.H. Sachtler, J. Phys. Chem. 96 (1992) 7733.
[38] F. Fajardie, J.-F. Tempère, J.-M. Manoli, O. Touret, G. Blanchard, G. Djéga-Mariadassou, J. Catal. 179 (1998) 469.